CFD Simulation of Transonic Flow Through the Tip-Section Turbine Blade Cascade Intended for the Long Turbine Blade

Pavlo Kosiak[1,*], *Jindřich* Hála[1], *Martin* Luxa[1], and *Jaromír* Příhoda[1]

[1]Institute of Thermomechanics of the Czech Academy of Sciences, Dolejškova 5, 182 00 Prague 6, Czech Republic

Abstract. The paper deals with numerical simulations of transonic flow through the turbine blade cascade consisting of flat profiles. The cascade is one of variants of the tip section of ultra-long blades, which were designed for the last stage of the steam turbine. CFD simulations were realized by means of the ANSYS CFX commercial software using the γ-Re_θ bypass transition model completed by the two-equation SST turbulence model. Some simulations were made only by the SST turbulence model for comparison. Numerical results were compared with experimental data. Calculations performed for two nominal regimes and two computational domains. In addition to the standard computational domain, the calculation was performed for a domain with an extended output part for the suppression of reflected shock waves. The interaction of the inner branch of the exit shock wave with the boundary layer on the blade suction side leads in the both flow regimes to the flow separation followed by the transition to turbulence. The flow structure in the blade cascade obtained for the extended domain corresponds well to experimental results.

Keywords: *CFD simulation*, *tip-section blade cascade, flat profile, shock-wave/boundary-layer interaction*

1 Introduction

The last stages of the steam turbine have a significant impact on the total efficiency of the turbine, see Luxa [1]. Therefore, the considerable attention is paid especially to the flow through the tip sections of the last stage. The compressible flow through the tip section of the blade cascade has a transonic character with shock-waves in the flow field. The form of the tip/section blades is designed not only from viewpoint of aerodynamics but also from viewpoint of dynamics and vibration. These conditions have resulted to the design of flat blade profiles which are relatively sensitive to the angle of attack. This leads to the design of flat blades profiles that are relatively sensitive to the angle of attack. As follows from simulations of Musil et al. [2], the inlet angle has a strong influence on the inlet Mach number and for some regimes even a small change of the inlet angle changes the flow from the transonic to the supersonic character.

* Corresponding author: kosiak@it.cas.cz

The flow field in the cascade is then significantly influenced by the interaction of shock waves with the boundary layer, especially by the interaction of the inner branch of the exit shock wave with the boundary layer on the suction side of the blade (see Luxa et al. [3]). The shock-wave/boundary-layer interaction is important for the flow structure including the losses in the blade cascade, see Ligrani et al. [4]. A long-term research is devoted to this problem, but mainly on the interaction of the shock wave with the turbulent boundary layer. Ganapathisubramani et al. [5] dealt with the effect of the upstream boundary layer on the shock-induced separation. Giepman et al. [6] realized experimental investigation of the laminar and transitional oblique shock wave reflections for a range of Mach numbers.

This paper deals with the numerical simulation of the 2D compressible flow through the TR-U-9 blade cascade which presents one of variants of last-stage tip section blades. The blade cascade has been designed for two nominal regimes with the subsonic inlet Mach number M_1 = 0.8 and the outlet isentropic Mach numbers M_{2is} = 1.6 and 1.8 respectively. The CFD simulation was performed by means of the ANSYS CFX commercial software for the both regimes using two different computational domains. Numerical results are compared with experimental data of Luxa et al. [7].

2 Numerical simulations

Simulations of compressible flows were completed by the conditionally-averaged Navier-Stokes equations completed by constitutional relations for the ideal gas, the two-equation SST turbulence model of Menter [8] and by the bypass-transition γ-$Re_{\theta t}$ model of Langtry and Menter [9].

The transition model is based on transport equations for the intermittency coefficient and the local transition momentum Reynolds number. The intermittency coefficient is given by the equation

$$\frac{\partial(\rho\gamma)}{\partial t}+\frac{\partial(\rho\overline{U_j}\gamma)}{\partial x_j}=P_\gamma-E_\gamma+\frac{\partial}{\partial x_j}\left[\left(\mu+\frac{\mu_t}{\sigma_\gamma}\right)\frac{\partial\gamma}{\partial x_j}\right] \tag{1}$$

The production term

$$P_\gamma=F_{length}C_{a1}\rho S(\gamma F_{onset})^{\frac{1}{2}}(1-C_{e1}\gamma) \tag{2}$$

contains empirical correlations F_{onset} for the transition onset and F_{length} for the transition length. The destruction term E_γ allows the prediction of the relaminarization of the boundary layer during a strong acceleration of the flow. The empirical correlation for the transition onset F_{onset} depends on the critical Reynolds number $Re_{\theta c}$ giving the position where the turbulent energy begins to grow up. The onset and length of the transition region, i.e. parameters $Re_{\theta c}$ and L_{length} are expressed by means of the local Reynolds number $\widetilde{Re_{\theta t}}$ The application of local variables is allowed by the relation between the Reynolds number related to the momentum thickness and the maximum of the vorticity Reynolds number used in the form $Re_\theta = Re_{vmax}/2.193$ valid for the Blasius boundary layer. The parameters $Re_{\theta c}$ and L_{length} are expressed by means of the local Reynolds number $\widetilde{Re_{\theta t}}$ given by the transport equation

$$\frac{\partial(\rho\widetilde{Re_{\theta t}})}{\partial t}+\frac{\partial(\rho U_j\widetilde{Re_{\theta t}})}{\partial x_j}=P_{\theta t}+\frac{\partial}{\partial x_j}\left[\sigma_{\theta t}(\mu+\mu_t)\frac{\partial\widetilde{Re_{\theta t}}}{\partial x_j}\right] \tag{3}$$

The model is switched over to a simple algebraic transition model in the case of the transition in separated flow. The effective value of the intermittency coefficient is given by the relation

$$\gamma_{eff}=max(\gamma,\gamma_{sep}) \tag{4}$$

Due to local variables the transition model can be used for the simulation of complex flows using unstructured computational grids. Calculations were realized by means of the ANSYS CFX commercial software.

Numerical simulation of flow through blade cascades are usually conducted using the computational domain corresponding to one pitch of the cascade with the inlet and the outlet in the distance about one half of the pitch from the leading and trailing edges respectively, see e. g. Cutrone et al. [10] and/or Louda et al. [11]. The outlet isentropic Mach number corresponds to the mean value of the static pressure in the traversing plane situated in a relatively short distance downstream the cascade. The other possibility is the application of the domain corresponding to the experimental arrangement of the test section in the wind tunnel (see Louda and Příhoda [12]). The computational domain covers a part of the inlet channel, the test section with the blade cascade and the prismatic section of settling chamber. However, this treatment puts greater demands on the computational technique.

The acceptable results can be as well achieved by the application of the extended outlet part of the computational domain with the prescription of the outlet static pressure corresponding to the pressure in the settling chamber behind the test section. The computational domain and mesh were created in two variants using GMSH free software. The scheme of the domain is shown in Fig. 1. The width is one pitch of the blade cascade. The both domains differ is the length of the outlet region. The short domain has the outlet length 1.78*s* while the extended one one has the outlet length 4*s*. Two computational domains with different outlet parts were used because of the study the effect of non-physical parasitic shock waves, which originates as reflection waves at the outlet boundary of the computational domain and might influence the flow field in the inter-blade channel.

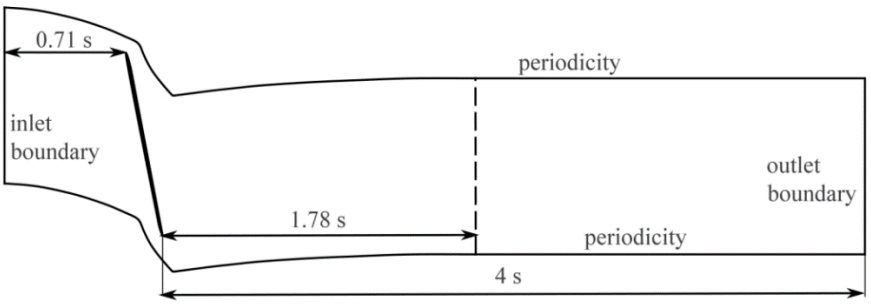

Fig. 1. Computational domain.

The computational domain consists of two grids - the structured O grid with quadrilateral cells around the blade and the triangular grid in the rest of the domain. The detail of the grid near to the trailing edge is shown in Fig. 2. The short domain contains about 167000 triangular cells and 54500 quadrilateral cells while the extended domain has 379000 triangular cells and 63000 quadrilateral cells. The grid has 665 nodes on the pressure side and 650 nodes on the suction side. The grid is refined near the wall with the first node in the distance $y^+ \approx 0.5$ from the wall. Due to used software the domain has one cell in the z direction.

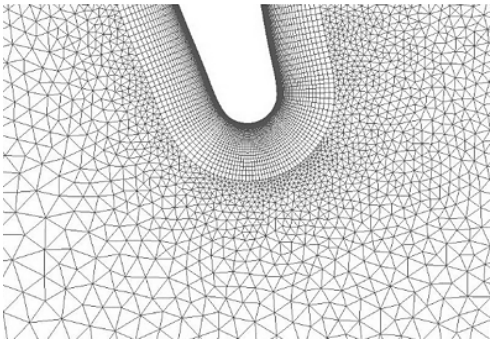

Fig. 2. Detail of the grid close to the trailing edges.

Numerical simulations were carried out for two nominal regimes characterized by the outlet isentropic Mach number M_{2is} = 1.6 and 1.8. Boundary conditions are the same for the both computational domain. The inlet boundary conditions are prescribed by the total pressure, the flow angle and by turbulence parameters, i.e. the turbulence level Tu = 10 % and the ratio of turbulent and molecular viscosity μ_t/μ = 250. The outlet boundary condition is given by the static pressure in accordance with the Mach number in the settling chamber behind the test section with the blade cascade. The turbulence intensity upstream the blade cascade $Tu \approx 1.5$ % corresponds to measured values at Mach number $M_1 \approx 0.8$. The periodic boundary condition is used on side boundaries of the computation domain.

3 Results

The TR-U-9 blade cascade consists of flat profiles with shaped leading and trailing parts. The cascade has the profile chord c = 0.15 m, the relative pitch s/c = 0.904, the maximum relative thickness $t/c \approx 0.02$ and the stagger angle γ = 79.23°measured from the blade suction side. Similarly, as for other tip-section blade cascades pressure and suction sides are on the inverse blade sides than usually. All simulations were realized according to experiments with the inlet angle α_1 = 79.23°. Experiments covering optical (interferometry and schlieren technique) and pneumatic measurements were accomplished in the in the suction-type high-speed wind tunnel in the Aerodynamic laboratory of the Institute of Thermomechanics at Nový Knín. The Mach-Zehnder interferometer was used for optical measurements. Pneumatic measurements were realized by the Prandtl probe upstream the blade cascade and by the five-hole conical probe in the traversing plane behind the blade cascade. A more detailed description is given e. g. by Luxa et al. [7].

The structure of the flow through the tip-section turbine blade cascade considerably depends on the character of the shock-wave/boundary-layer interaction. This interaction is usually related to the flow separation followed by the transition in separated flow in the case of the laminar boundary layer. The interferometric and schlieren pictures of the flow field for the Mach number M_{2is} = 1.8 are shown in Fig. 3.

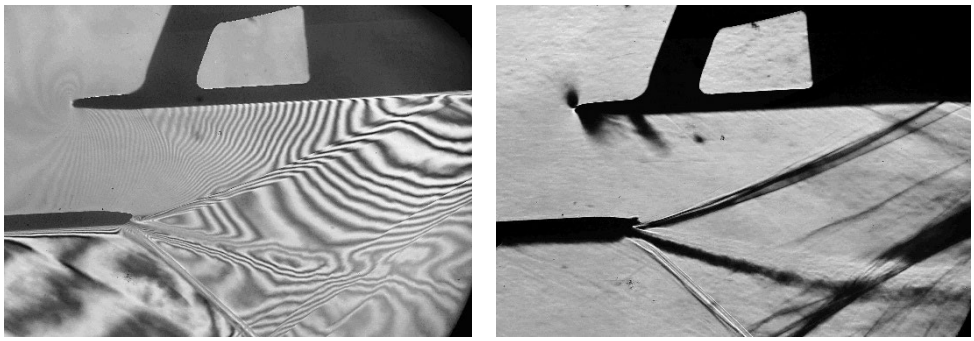

a) Interferometric picture b) Schlieren picture

Fig. 3. Flow field for the Mach number M_{2is} = 1.8.

The effect of the interaction of the inner branch of the exit shock wave of the neighboring blade with the boundary layer on the suction side of the blade is well apparent in the interferometric and schlieren pictures.

The corresponding calculated field of Mach isolines is shown in Fig. 4 for the both computational domains. The flow field in the inter-blade channel is considerably influenced by the interaction of the inner branch of the exit shock wave of the neighboring blade with the boundary layer on the suction side of the blade. This is evident both from interferometric pictures and from the computed field of the Mach isolines. As can be seen in Fig. 4a), the field of Mach isolines obtained for the short domain contains a parasitic shock wave reflected from the domain boundary. Due to the extension of the outlet part of the domain the effect of parasitic shock wave is negligible and so only the results for the extended domain are presented.

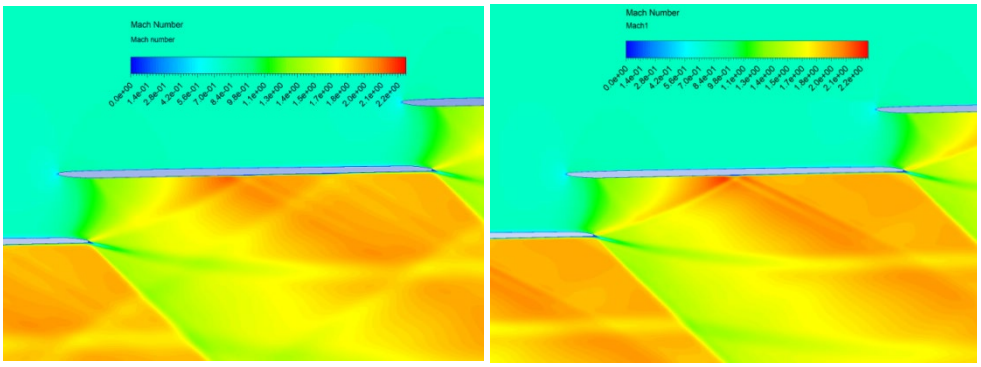

a) Short computational domain b) Long computational domain

Fig. 4. Field of the Mach number isolines for M_{2is} = 1.8.

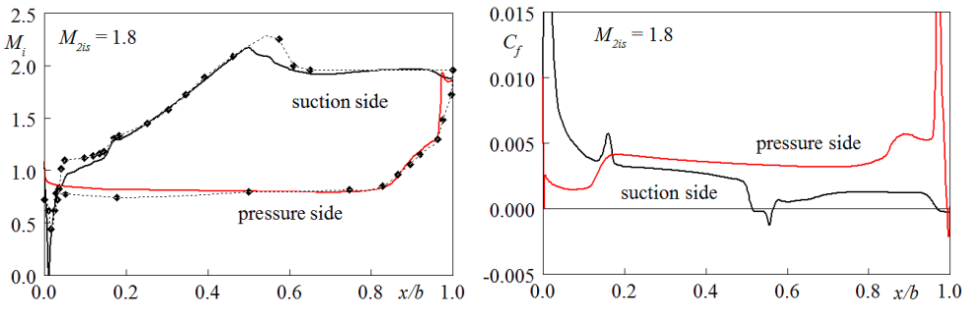

a) Isentropic Mach number b) Skin friction coefficient

Fig. 5. The distribution of the isentropic Mach number and the skin friction coefficient for M_{2is} = 1.8.

The distribution of the isentropic Mach number M_i on the blade profile for the Mach number M_{2is} = 1.8 is shown in Fig. 5a). Experimental results were evaluated from interferogram results. The so-called pressure and suction sides are for the tip-section cascades ordinarily on the inverse blade sides due to the stagger angles. The skin friction distribution is expressed in the Fig. 5b) by the coefficient C_f given by the ratio of the wall friction and the inlet dynamics pressure.

The structure of the flow field in the inter-blade channel depends largely on the interaction of the inner branch of the exit shock wave of the neighboring blade with the boundary layer on the suction side of the blade. It follows from interferometric pictures and from the computed field of the Mach isolines as well. The flow on the suction side accelerates from the leading edge up to the shock-wave interaction. The effect of the

sudden change of the blade surface curvature can be seen at $x/b \approx 0.15$ where the curved leading part passes into the flat-plate profile. On the pressure side the velocity is mostly constant corresponding to the flow around the flat plate.

It can be seen from the interferometric picture and the isentropic Mach number distribution that the shock-wave interaction with the boundary layer takes place at the distance $x/b \approx 0.55$ where b is the axial chord of the blade. According to numerical simulations the position of the interaction is shifted somewhat upstream in the comparison with experimental results to the distance about $x/b \approx 0.51$. The distribution of the skin friction coefficient corresponds to the isentropic Mach number on the blade. On the suction side, there is obvious the effect of the sudden change in the surface curvature corresponding to changes in the Mach number. The interaction with the shock wave leads to the flow separation followed by the transition in the separated flow and the reattachment. The detail of the velocity field in the position of the shock-wave interaction for the $M_{2is} = 1.8$ is shown in Fig. 6. The reverse flow, forming a short separated region, can be seen near the wall.

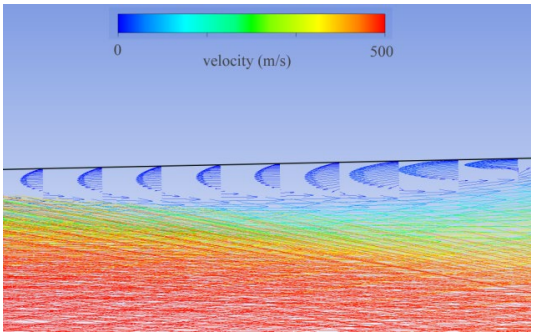

Fig. 6. Velocity field in the position of the shock-wave interaction.

However, it follows from the interferometric and hot-film measurements (see Luxa et al. [7]) that the transition on the suction side could occur in the attached flow upstream the interaction of the boundary layer with the shock wave. The velocity peak near the leading edge induces a very short laminar separation bubble on the pressure side. According to the simulation with the transition model the transition in attached flow occurs on the pressure side at the distance $x/b = 0.1$ from the leading edge. A great increase of C_f followed by the separation just upstream the trailing edge.

The distribution of the skin friction coefficient for the Mach number $M_{2is} = 1.8$ and for the numerical simulation by means of the turbulence model without the transition model is shown in Fig. 7. The course of the skin friction coefficient is similar as for the calculation with the transition model. On the pressure side, the coefficient C_f gradually decreases from the leading edge and for $x/b > 0.3$ corresponds to the calculation with the transition model. Also on the suction side, the course of the C_f is similar. However, there is no separation at the interaction of the shock wave with the turbulent boundary layer. As well, values of the skin friction coefficient on the suction side are

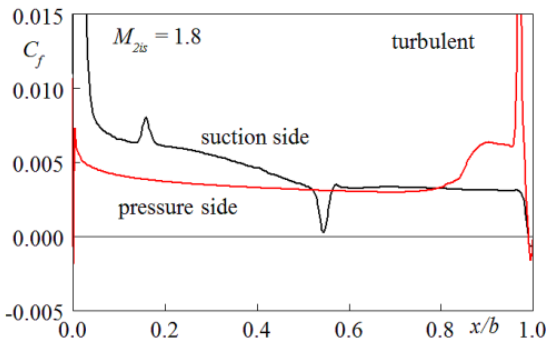

Fig. 7. Distribution of the skin friction coefficient for $M_{2is} = 1.8$ (turbulent model only).

higher. The supersonic expansion arises on the pressure side upstream of the asymmetric trailing edge. The near wake is shifted in the suction side direction and the inlet part of exit shock wave is very thick. The significant supersonic flow deviation takes place downstream the trailing edge, see Fig. 8. It leads to a short flow separation on the both blade sides.

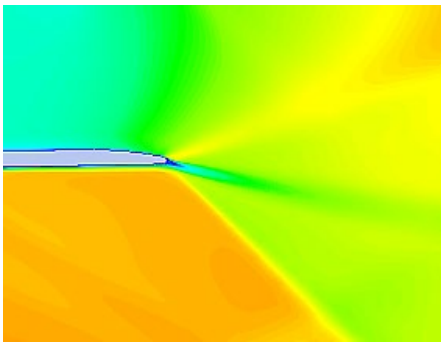

Fig. 8. Detail of the Mach number isolines near the trailing edge for M_{2is} = 1.8.

The investigation of the flow through the blade cascade at the Mach number M_{2is} = 1.6 was accomplished in the same experimental configuration. The interferometric and schlieren pictures of the flow field are shown in Fig. 9. The calculated field of Mach isolines for M_{2is} = 1.6 and the extended computational domain is shown in Fig. 10.

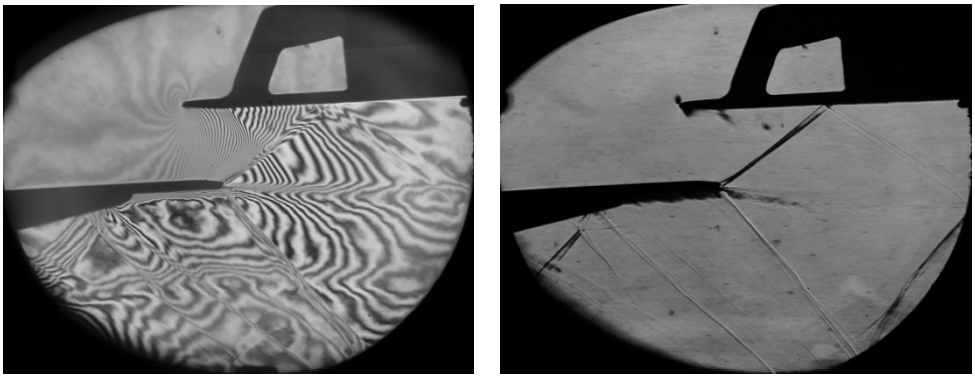

a) Interferometric picture b) Schlieren picture

Fig. 9. Flow field for the Mach number M_{2is} = 1.6.

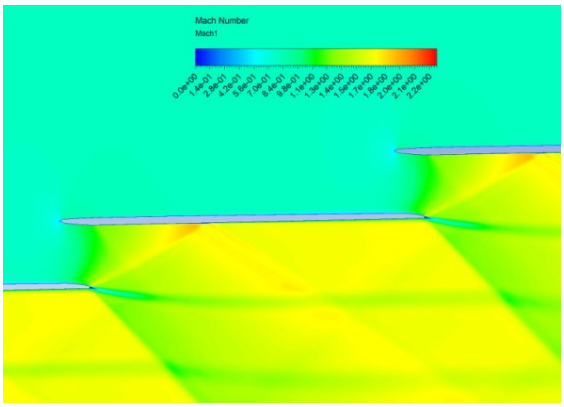

Fig. 10. Field of the Mach number isolines for M_{2is} = 1.6.

As can be seen from Fig. 10, the flow field for M_{2is} = 1.6 is very similar to the field for M_{2is} = 1.8, only the differences of Mach numbers are not so noticeable. The decisive influence on the flow structure in the inter-blade channel has again the interaction of the inner branch of the exit shock wave with the boundary layer on the suction side of the blade. The value of the outlet Mach number affects mainly the angle of the output shock wave. As the Mach number increases, this angle decreases. This leads to a shift in the position of the shock-wave/boundary-layer interaction with the increasing Mach number downstream towards the trailing edge.

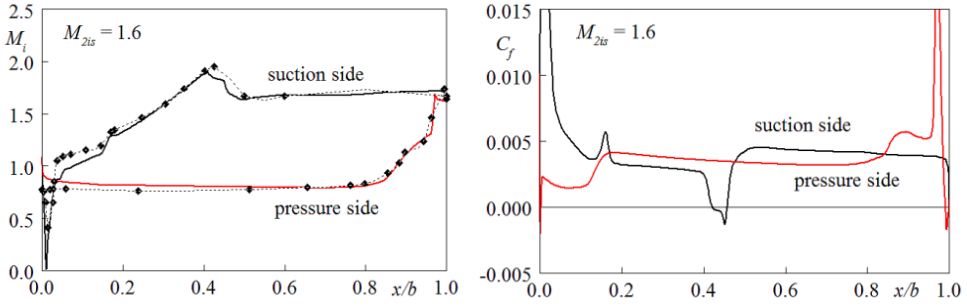

a) Isentropic Mach number b) Skin friction coefficient

Fig. 11. The distribution of the isentropic Mach number and the skin friction coefficient for M_{2is} = 1.6.

The distribution of the isentropic Mach number and the skin friction coefficient for M_{2is} = 1.6 shown in Fig. 11 practically corresponds to the results for M_{2is} = 1.8. There is only a decrease in the Mach number M_i on the trailing edge from the value of M_i = 1.96 to M_i = 1.66. The transition onset on the pressure side is for the Mach number M_{2is} = 1.6 at the distance x/b = 0.1 as well as for the higher value M_{2is}. The position of the interaction of the shock wave with the boundary layer is shifted from x/b = 0.55 for the lower Mach number M_{2is} = 1.6 to the distance x/b = 0.425. The flow separation and the transition in the detached flow on the suction side of the profile are shifted in the same way.

4 Conclusions

Numerical simulations of 2D transonic flow through the turbine blade cascade consisting of flat profiles were realized. The cascade is one of variants of the tip section of ultra-long blades, which were designed for the last stage of the steam turbine. CFD simulations were realized by means of the ANSYS CFX commercial software using the γ-$Re_{\theta t}$ bypass transition model completed by the two-equation SST turbulence model. Some simulations were made only by the SST turbulence model for comparison. Numerical results were compared with experimental data. Calculations were carried out for two nominal regimes and two computational domains. In addition to the standard computational domain, the calculation was performed for a domain with an extended output part for the suppression of reflected shock waves. Due to the blade profile, the flow near the leading edge on the pressure side can be influenced by the short laminar separation bubble. Similarly, a short flow separation occurs just upstream the asymmetric trailing edge.

The interaction of the inner branch of the exit shock wave with the boundary layer on the blade suction side leads in the both flow regimes to the flow separation followed by the transition to turbulence. This shock-wave/boundary-layer interaction with flow separation and the transition in the detached flow on the suction side of the profile are shifted downstream with increasing outlet isentropic Mach number M_{2is}. For the extended

computational domain the agreement of numerical simulations with experimental data is acceptable.

This research was supported by the Czech Science Foundation (GACR) under the grant No. 20-11537S. Institutional support RVO 61388998 is also gratefully acknowledged. Institutional support RVO 61388998 is also gratefully acknowledged.

References

1. Luxa, M. (2017). *Effects of the design of the last-stage rotor of the low-pressure part of the high-power steam turbine with very long blades on the transonic flow field,* Habilitation Thesis, Czech Technical University in Prague, Prague, (in Czech)
2. Musil, J., Příhoda, J., Fürst, J. (2019). Simulation of supersonic flow through the tip-section turbine blade cascade with a flat profile, *Proc. Conference Topical Problems of Fluid Mechanics 2019,* Prague, 169-174, 2019, https://doi.org/10.14311/TPFM.2019.023
3. Luxa, M., Příhoda, J., Šimurda, D., Straka, P., Synáč, J. (2016). Investigation of the compressible flow through the tip-section turbine blade cascade with supersonic inlet, *Journal of Thermal Science,* 25, 2, s. 138-144, https://doi.org/10.1007/s11630-016-0844-0
4. Ligrani, P. M., McNabb, E. S., Collopy H., Anderson, M., Marko, S. M. (2020). Recent investigations of shock wave effects and interactions, *Advances in Aerodynamics*, 2, 4, 23 p., https://doi.org/10.1186/s42774-020-0028-1
5. Ganapathisubramani, B., Clemens, N. T., Dolling, D. S. (2007). Effects of upstream boundary layer on the unsteadiness of shock-induced separation, *Journal Fluid Mechanics*, 585, 369-394, https://doi.org/10.1017/S0022112007006799
6. Giepman, R. H. M., Schrijer, F. F. J., Oudheusden van, B. W. (2015). High-resolution PIV measurements of a transitional shock wave–boundary layer interaction, *Experiments in Fluids,* 56, 1-20, https://doi.org/10.1007/s00348-015-1977-8
7. Luxa, M., Šimurda, D., Hála, J. (2020). *Measurements on TR-U-9 cascade*, Institute of Thermomechanics, Czech Academy of Sciences, Prague, Research Report Z1610/2020
8. Menter, F. (1994). Two-equation eddy-viscosity turbulence model for engineering applications, *AIAA Journal,* 32, 1598-1605, https://doi.org/10.2514/3.12149
9. Langtry, R. B., Menter, F. R. (2009). Correlation-based transition modeling for unstructured parallelized computational fluid dynamics codes, *AIAA Journal,* 47, 2894-2906, https://doi.org/10.2514/1.42362
10. Cutrone, L., De Palma, P., Pascazio, G., Napolitano, M. (2007). An evaluation of bypass transition models for turbomachinery flows, *International Journal of Heat and Fluid Flow*, 28, 161-177, http://doi:10.1016/j.ijheatfluidflow.2006.02.031
11. Louda, P., Straka, P., Příhoda, J. (2018). Simulation of transonic flows through a turbine blade cascade with various prescriptions of outlet boundary condition, *EPJ Web of Conferences*, 180, 02056, 6 p., https://doi.org/10.1051/epjconf/201818002056
12. Louda, P., Příhoda, J. (2021). Study on the numerical model of transonic wind tunnel test section, *Journal of Thermal Science*, 30, 231-241, https://doi.org/10.1007/s11630-020-1277-3